

# Tunneling of Electrons in Graphene via Double Triangular Barrier in External Fields

Miloud Mekkaoui<sup>a</sup>, Ahmed Jellal<sup>\*a,b</sup> and Hocine Bahlouli<sup>c</sup>

<sup>a</sup>*Laboratory of Theoretical Physics, Faculty of Sciences, Chouaib Doukkali University,  
PO Box 20, 24000 El Jadida, Morocco*

<sup>b</sup>*Canadian Quantum Research Center, 204-3002 32 Ave Vernon,  
BC V1T 2L7, Canada*

<sup>c</sup>*Physics Department, King Fahd University of Petroleum & Minerals,  
Dhahran 31261, Saudi Arabia*

## Abstract

We study the transmission probability of Dirac fermions in graphene scattered by a triangular double barrier potential in the presence of an external magnetic field. Our system made of two triangular potential barrier regions separated by a well region characterized by an energy gap. Solving our Dirac-like equation and matching the solutions at the boundaries allowed us to express our transmission and reflection coefficients in terms of transfer matrix. We show in particular that the transmission exhibits oscillation resonances that are manifestations of the Klein tunneling effect. The triangular barrier electrostatic field was found to play a key role in controlling the peak of tunneling resistance. However, it only slightly modifies the resonances at oblique incidence and leaves Klein paradox unaffected at normal incidence.

PACS numbers: 72.80.Vp, 73.21.-b, 71.10.Pm, 03.65.Pm

Keywords: graphene, double barriers, scattering, transmission.

---

\*ajellal@ictp.it – a.jellal@ucd.ac.ma

# 1 Introduction

Graphene [1] remains among the most fascinating and attractive subjects in contemporary condensed matter physics. This is because of its exotic physical and transport properties and the apparent similarity of its mathematical model to the one describing massless relativistic fermions in two dimensions. As a consequence of this relativistic-like behavior, particles could tunnel through very high barriers in contrast to the conventional tunneling of non-relativistic particles, an effect known in relativistic field theory as Klein tunneling. This tunneling effect has already been observed experimentally [2] in graphene systems. However, there are various ways for creating barrier structures in graphene [3, 4]. For instance, it can be realized by applying a gate voltage, cutting the graphene sheet into a finite width to create a nanoribbons, using doping or through the creation of a magnetic barrier. In the case of graphene, results of the transmission coefficient and the tunneling conductance were already reported for the electrostatic barriers [5–7], magnetic barriers [6, 8, 9], potential barrier [10], linear [11] and triangular [12] barriers.

One of the present author [10] theoretically studied the electronic transport properties of Dirac fermions through one and double triangular barriers in graphene nanoribbon. The transmission, conductance and Fano factor are obtained to be various parameters dependent such as well width, barrier height and barrier width. Therefore, different discussions are given and comparison with the previous significant works is done. In particular, it is shown that at Dirac point the Dirac fermions always own a minimum conductance associated with a maximum Fano factor and change their behaviors in an oscillatory way (irregularly periodical tunneling peaks) when the potential of applied voltage is increased.

In our present work we study the transmission probability of Dirac fermions in graphene scattered by a triangular double barrier potential in the presence of a uniform magnetic fields  $B$  confined to the well region between the two barriers. We emphasis that  $B$ -field discussed in our manuscript is applied externally and is perpendicular to the graphene sheet. It can be created for instance by depositing a type-I superconducting film on top of the system except for a strip  $|x| < d_1$  which is isolated in order to apply a perpendicular magnetic field in its domain. This patterning technique of creating the desired magnetic field profile was proposed in [13]. One of the interesting features of such a magnetic field profile is that it can bind electrons, contrary to the usual potential step profile. Such a step magnetic field will indeed result in electron states that are bound to the step  $B$ -field and that move in one direction along the step. Thus there is a current along the  $y$ -direction but it is a very small effect and is not relevant for our problem (those electrons have  $k_x = 0$ ). Indeed, we consider free electron states that have in general non zero  $k_x$ , because otherwise they will not tunnel. A recent work studied double barriers with magnetic field in graphene without mass term [14].

The paper is organized as follows. In section 2, we formulate our model by setting the Hamiltonian system describing particles scattered by a triangular double barrier whose well potential zone is subject to a magnetic field in the presence of a mass term. In section 3, we consider the case of static double barriers and derive the energy spectrum to finally determine the transmission and reflection probabilities. Their behaviors are numerically investigated and in particular resonances were seen in different regions while Klein tunneling was observed to persist at normal incidence. In section 4, we study the same system but this time taking into account the presence of a uniform magnetic field

confined to the barrier region. Using boundary conditions, we split the energy into three domains and then calculate the transmission probability in each case. In each situation, we discuss the transmission resonances that characterize each region and stress the importance of our results. We conclude our work in the final section.

## 2 System setting

Our system is a flat sheet of graphene subject to the barrier  $V(x) = V_j$  along the  $x$ -direction while particles are free in the  $y$ -direction and a mass term is applied in region 3 as graphically represented in Figure 1. Formally, we have regions  $j = 1, \dots, 5$  characterized by the electrostatic potential

$$V(x) = \begin{cases} \Lambda(d_2 + \gamma x), & d_1 \leq |x| \leq d_2 \\ V_2, & |x| \leq d_1 \\ 0, & \text{otherwise} \end{cases} \quad (1)$$

where  $\gamma = 1$  for  $x \in [-d_2, -d_1]$ ,  $\gamma = -1$  for  $x \in [d_1, d_2]$  and the parameter  $\Lambda = \frac{V_1}{d_2 - d_1}$  gives the slope of triangular potentials which represents the strength of the applied electrostatic field.

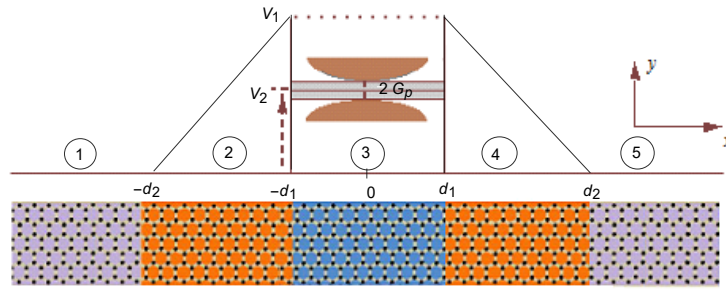


**Figure 1** – Schematic diagram for the monolayer graphene double barrier.

The Hamiltonian system can be written as

$$H = v_F \boldsymbol{\sigma} \cdot \left( \mathbf{p} + \frac{e}{c} \mathbf{A} \right) + V(x) \mathbb{I}_2 + G_p \Theta(d_1^2 - x^2) \sigma_z \quad (2)$$

with the Fermi velocity  $v_F \approx 10^6 m/s$ , the Pauli matrices  $\sigma_i$  in pseudospin space, the momentum operator  $\mathbf{p} = (p_x, p_y)$ , the  $2 \times 2$  unit matrix  $\mathbb{I}_2$  and  $\Theta$  is the Heaviside step function. The vector potential associated to perpendicular constant magnetic field  $B$  will be chosen the Landau gauge  $\mathbf{A} = (0, Bx)$ . The energy gap  $G_p = mv_F^2$  is originating from the sublattice symmetry breaking, which also can be seen as  $G_p = G_{p,so}$  originating from spin-orbit interaction.

## 3 Static double barrier

### 3.1 Energy spectrum: electrostatic double barrier

We consider a Hamiltonian describing Dirac fermions in graphene scattered by an electrostatic double barrier potential in the absence of magnetic field,  $\mathbf{A} = 0$ . In this case (2) reduces to

$$H_s = v_F \boldsymbol{\sigma} \cdot \mathbf{p} + V(x) \mathbb{I}_2 + G_p \Theta(d_1^2 - x^2) \sigma_z \quad (3)$$

where  $j$  labels the five regions indicated schematically in Figure 1 showing the space configuration of the potential profile. Due to inversion and time reversal symmetries we therefore need to study our system only near the  $\mathbf{K}$  point. The time-independent Dirac equation for the spinor  $\Phi(x, y) = (\varphi^+, \varphi^-)^T$  at energy  $E = v_F \epsilon$  then reads, in unit system  $\hbar = m = c = 1$ , as

$$[\boldsymbol{\sigma} \cdot \mathbf{p} + v_j \mathbb{I}_2 + \mu \Theta (d_1^2 - x^2) \sigma_z] \Phi(x, y) = \epsilon \Phi(x, y) \quad (4)$$

where  $V_j = v_F v_j$  and  $G_p = v_F \mu$ . Our system is supposed to have finite width  $W$  with infinite mass boundary conditions on the wavefunction at the boundaries  $y = 0$  and  $y = W$  along the  $y$ -direction [15, 16]. These boundary conditions result in a quantization of the transverse momentum along the  $y$ -direction as

$$k_y = \frac{\pi}{W} \left( n + \frac{1}{2} \right), \quad n = 0, 1, 2, \dots \quad (5)$$

One can therefore assume a spinor solution of the following form  $\Phi_j = (\varphi_j^+(x), \varphi_j^-(x))^T e^{ik_y y}$  and the subscript  $j = 1, 2, 3, 4, 5$  refers to the space region while the superscripts indicate the two spinor components. Solving the eigenvalue equation to obtain the upper and lower components of the eigenspinor in the incident and reflection region 1 ( $x < -d_2$ ) gives

$$\Phi_1 = \begin{pmatrix} 1 \\ z_1 \end{pmatrix} e^{i(k_1 x + k_y y)} + r_{s,n} \begin{pmatrix} 1 \\ -z_1^{-1} \end{pmatrix} e^{i(-k_1 x + k_y y)}, \quad z_1 = s_1 \frac{k_1 + ik_y}{\sqrt{k_1^2 + k_y^2}} \quad (6)$$

associated to the dispersion relation  $\epsilon = s_1 \sqrt{k_1^2 + k_y^2}$  with  $s_j = \text{sign}(E)$ .

In regions 2 and 4 ( $d_1 < |x| < d_2$ ), the general solution can be expressed in terms of the parabolic cylinder function [11, 17, 18] as

$$\chi_\gamma^+ = c_{n1} D_{\nu_n-1}(Q_\gamma) + c_{n2} D_{-\nu_n}(-Q_\gamma^*) \quad (7)$$

where  $c_{n1}$  and  $c_{n2}$  are constants,  $\nu_n = \frac{ik_y^2}{2\varrho}$  and  $Q_\gamma(x) = \sqrt{\frac{2}{\varrho}} e^{i\pi/4} (\gamma \varrho x + \epsilon_0)$ , with  $\epsilon_0 = \epsilon - v_1$ ,  $\Lambda = v_F \varrho$ ,  $V_1 = v_F v_1$ . The lower spinor component is given by

$$\chi_\gamma^- = -\frac{c_{n2}}{k_y} \left[ 2(\epsilon_0 + \gamma \varrho x) D_{-\nu_n}(-Q_\gamma^*) + \sqrt{2\varrho} e^{i\pi/4} D_{-\nu_n+1}(-Q_\gamma^*) \right] - \frac{c_{n1}}{k_y} \sqrt{2\varrho} e^{-i\pi/4} D_{\nu_n-1}(Q_\gamma). \quad (8)$$

The components of the spinor solution of the Dirac equation (3) in regions 2 and 4 can be obtained from (7) and (8) with  $\varphi_\gamma^+(x) = \chi_\gamma^+ + i\chi_\gamma^-$  and  $\varphi_\gamma^-(x) = \chi_\gamma^+ - i\chi_\gamma^-$ . Then, in regions 2 and 4 we have the eigenspinors

$$\Phi_j = a_{j-1} \begin{pmatrix} \eta_\gamma^+(x) \\ \eta_\gamma^-(x) \end{pmatrix} e^{ik_y y} + a_j \begin{pmatrix} \xi_\gamma^+(x) \\ \xi_\gamma^-(x) \end{pmatrix} e^{ik_y y} \quad (9)$$

where  $\gamma = \pm 1$  and we have set

$$\eta_\gamma^\pm(x) = D_{\nu_n-1}(Q_\gamma) \mp \frac{1}{k_y} \sqrt{2\varrho} e^{i\pi/4} D_{\nu_n}(Q_\gamma) \quad (10)$$

$$\xi_\gamma^\pm(x) = \pm \frac{1}{k_y} \sqrt{2\varrho} e^{-i\pi/4} D_{-\nu_n+1}(-Q_\gamma^*) \pm \frac{1}{k_y} (-2i\epsilon_0 \pm k_y - \gamma 2i\varrho x) D_{-\nu_n}(-Q_\gamma^*). \quad (11)$$

In region 3, we use (3) to obtain the eigenspinor

$$\Phi_3 = b_1 \begin{pmatrix} \alpha \\ \beta z_3 \end{pmatrix} e^{i(k_3 x + k_y y)} + b_2 \begin{pmatrix} \alpha \\ -\beta z_3^{-1} \end{pmatrix} e^{i(-k_3 x + k_y y)} \quad (12)$$

with the parameters

$$z_3 = s_3 \frac{k_3 + i k_y}{\sqrt{k_3^2 + k_y^2}}, \quad \alpha = \left(1 + \frac{\mu}{\epsilon - v_2}\right)^{1/2}, \quad \beta = \left(1 - \frac{\mu}{\epsilon - v_2}\right)^{1/2} \quad (13)$$

and the wave vector  $k_3 = \sqrt{(\epsilon - v_2)^2 - \mu^2 - k_y^2}$ ,  $s_3 = \text{sign}(\epsilon - v_2)$ . The eigenspinor in region 5 can easily be obtained

$$\Phi_5 = t_{s,n} \begin{pmatrix} 1 \\ z_1 \end{pmatrix} e^{i(k_1 x + k_y y)} \quad (14)$$

in similar way to region 1. These results will be embedded to deal with tunneling properties of our system.

### 3.2 Transmission and reflection: electrostatic double barrier

We determine the transmission and reflection probabilities for an electrostatic double barrier alone by requiring the continuity of the eigenspinor at junction interfaces. This yields

$$\Phi_1(-d_2) = \Phi_2(-d_2), \quad \Phi_2(-d_1) = \Phi_3(-d_1), \quad \Phi_3(d_1) = \Phi_4(d_1), \quad \Phi_4(d_2) = \Phi_5(d_2). \quad (15)$$

We prefer to express these relationships in terms of  $2 \times 2$  transfer matrices between different regions, then we write

$$\begin{pmatrix} a_j \\ b_j \end{pmatrix} = M_{j,j+1} \begin{pmatrix} a_{j+1} \\ b_{j+1} \end{pmatrix} \quad (16)$$

where  $M_{j,j+1}$  are the transfer matrices that couple the wavefunction in the  $j$ -th region to the wavefunction in the  $(j+1)$ -th region. Finally, we obtain the full transfer matrix  $M$  over the whole double barrier which can be written, in an obvious notation, as follows

$$\begin{pmatrix} 1 \\ r_{s,n} \end{pmatrix} = \prod_{j=1}^4 M_{j,j+1} \begin{pmatrix} t_{s,n} \\ 0 \end{pmatrix} = M \begin{pmatrix} t_{s,n} \\ 0 \end{pmatrix} \quad (17)$$

where  $M = M_{12} \cdot M_{23} \cdot M_{34} \cdot M_{45}$  is given by

$$M = \begin{pmatrix} m_{11} & m_{12} \\ m_{21} & m_{22} \end{pmatrix} \quad (18)$$

and the remaining matrices read as

$$M_{12} = \begin{pmatrix} e^{-ik_1 d_2} & e^{ik_1 d_2} \\ z_1 e^{-ik_1 d_2} & -z_1^* e^{ik_1 d_2} \end{pmatrix}^{-1} \begin{pmatrix} \eta_1^+(-d_2) & \xi_1^+(-d_2) \\ \eta_1^-(-d_2) & \xi_1^-(-d_2) \end{pmatrix} \quad (19)$$

$$M_{23} = \begin{pmatrix} \eta_1^+(-d_1) & \xi_1^+(-d_1) \\ \eta_1^-(-d_1) & \xi_1^-(-d_1) \end{pmatrix}^{-1} \begin{pmatrix} \alpha e^{-ik_3 d_1} & \alpha e^{ik_3 d_1} \\ \beta z_3 e^{-ik_3 d_1} & -\beta z_3^* e^{ik_3 d_1} \end{pmatrix} \quad (20)$$

$$M_{34} = \begin{pmatrix} \alpha e^{ik_3 d_1} & \alpha e^{-ik_3 d_1} \\ \beta z_3 e^{ik_3 d_1} & -\beta z_3^* e^{-ik_3 d_1} \end{pmatrix}^{-1} \begin{pmatrix} \eta_{-1}^+(d_1) & \xi_{-1}^+(d_1) \\ \eta_{-1}^-(d_1) & \xi_{-1}^-(d_1) \end{pmatrix} \quad (21)$$

$$M_{45} = \begin{pmatrix} \eta_{-1}^+(d_2) & \xi_{-1}^+(d_2) \\ \eta_{-1}^-(d_2) & \xi_{-1}^-(d_2) \end{pmatrix}^{-1} \begin{pmatrix} e^{ik_1 d_2} & e^{-ik_1 d_2} \\ z_1 e^{ik_1 d_2} & -z_1^* e^{-ik_1 d_2} \end{pmatrix}. \quad (22)$$

Consequently, the transmission and reflection amplitudes take the forms

$$t_{s,n} = \frac{1}{m_{11}}, \quad r_{s,n} = \frac{m_{21}}{m_{11}}. \quad (23)$$

Some symmetry relationship between the parabolic cylindric functions are worth mentioning, they are given by

$$\eta_{-1}^\pm(d_1) = \eta_1^\pm(-d_1), \quad \eta_{-1}^\pm(d_2) = \eta_1^\pm(-d_2) \quad (24)$$

$$\xi_{-1}^\pm(d_1) = \xi_1^\pm(-d_1), \quad \xi_{-1}^\pm(d_2) = \xi_1^\pm(-d_2). \quad (25)$$

We should point out at this stage that we were unfortunately forced to adopt a somehow cumbersome notation for our wavefunction parameters in different potential regions due to the relatively large number of necessary subscripts and superscripts. Before matching the eigenspinors at the boundaries, let us define the following shorthand notation

$$\eta_1^\pm(-d_1) = \eta_{11}^\pm, \quad \eta_1^\pm(-d_2) = \eta_{12}^\pm \quad (26)$$

$$\xi_1^\pm(-d_1) = \xi_{11}^\pm, \quad \xi_1^\pm(-d_2) = \xi_{12}^\pm. \quad (27)$$

After some lengthy algebra, one can solve the linear system given in (17) to obtain the transmission and reflection amplitudes in closed forms. As for the former one, we find

$$t_{s,n} = \frac{\alpha \beta e^{2i(k_1 d_2 + k_3 d_1)} (1 + z_1^2) (1 + z_3^2)}{z_3 (e^{4ik_3 d_1} - 1) (\alpha^2 \mathcal{Y}_2 + \beta^2 \mathcal{Y}_1) + \alpha \beta \mathcal{Y}_3} (\xi_{11}^+ \eta_{11}^- - \xi_{11}^- \eta_{11}^+) (\xi_{12}^- \eta_{12}^+ - \xi_{12}^+ \eta_{12}^-) \quad (28)$$

where we have defined the following quantities

$$\mathcal{Y}_1 = (\xi_{12}^- \eta_{11}^+ - \xi_{11}^+ \eta_{12}^- - \xi_{12}^+ \eta_{11}^+ z_1 + \xi_{11}^+ \eta_{12}^+ z_1) (\xi_{11}^+ \eta_{12}^+ + \xi_{11}^- \eta_{12}^- z_1 - \eta_{11}^+ (\xi_{12}^+ + \xi_{12}^- z_1)) \quad (29)$$

$$\mathcal{Y}_2 = (\xi_{11}^- \eta_{12}^+ - \xi_{11}^- \eta_{12}^- z_1 - \eta_{11}^- (\xi_{12}^+ + \xi_{12}^- z_1) (-\xi_{12}^- \eta_{11}^- + \xi_{12}^+ \eta_{11}^- z_1 - \xi_{11}^- (\eta_{12}^- + \eta_{12}^+ z_1)) \quad (30)$$

$$\mathcal{Y}_3 = \Gamma_0 (1 + z_1^2 z_3^2) + \Gamma_1 z_1 (1 - z_3) + \Gamma_2 (z_1^2 + z_3^2) + e^{4id_1 k_3} (\Gamma_3 + \Gamma_4) \quad (31)$$

together with

$$\Gamma_0 = -\xi_{12}^+ \xi_{12}^- \eta_{11}^+ \eta_{11}^- + \xi_{11}^+ \xi_{12}^- \eta_{11}^- \eta_{12}^+ + \xi_{11}^- \xi_{12}^+ \eta_{11}^+ \eta_{12}^- - \xi_{11}^+ \xi_{11}^- \eta_{12}^+ \eta_{12}^- \quad (32)$$

$$\Gamma_1 = (\xi_{12}^+)^2 \eta_{11}^+ \eta_{11}^- - (\xi_{12}^-)^2 \eta_{11}^+ \eta_{11}^- - \xi_{11}^- \xi_{12}^+ \eta_{11}^+ \eta_{12}^+ - \xi_{11}^+ \xi_{12}^- \eta_{11}^- \eta_{12}^- + \xi_{11}^+ \xi_{11}^- (\eta_{12}^+)^2 - \xi_{11}^+ \xi_{11}^- (\eta_{12}^-)^2 + \xi_{11}^- \xi_{12}^- \eta_{11}^+ \eta_{12}^- + \xi_{11}^+ \xi_{12}^- \eta_{11}^- \eta_{12}^+ \quad (33)$$

$$\Gamma_2 = \xi_{12}^+ \xi_{12}^- \eta_{11}^+ \eta_{11}^- - \xi_{11}^- \xi_{12}^- \eta_{11}^+ \eta_{12}^+ - \xi_{11}^+ \xi_{12}^+ \eta_{11}^- \eta_{12}^- + \xi_{11}^+ \xi_{11}^- \eta_{12}^+ \eta_{12}^- \quad (34)$$

$$\Gamma_3 = (\xi_{12}^+)^2 \eta_{11}^+ \eta_{11}^- (z_3^2 - 1) - \xi_{11}^- \xi_{12}^- \eta_{11}^+ [\eta_{12}^+ (1 + z_1^2 z_3^2) - \eta_{12}^- z_1 (z_3^2 - 1)] + \xi_{11}^- \xi_{11}^+ [(\eta_{12}^+)^2 z_1 - (\eta_{12}^-)^2 z_1 + \eta_{12}^+ \eta_{12}^- (z_1^2 - 1) (z_3^2 - 1)] \quad (35)$$

$$\Gamma_4 = \xi_{12}^- \eta_{11}^- [-\xi_{12}^- \eta_{11}^+ z_1 (z_3^2 - 1) + \xi_{11}^+ (\eta_{12}^- z_0 (z_3^2 - 1) + \eta_{12}^+ (z_1^2 + z_3^2))] + \xi_{12}^+ \xi_{12}^- \eta_{11}^+ \eta_{11}^- (z_1^2 + 1) (z_3^3 - 1) - \xi_{12}^+ \xi_{11}^+ \eta_{11}^- (\eta_{12}^- (1 + z_1^2 z_3^2) + \eta_{12}^+ z_1 (z_1^3 - 1)) + \xi_{12}^+ \xi_{11}^- [\eta_{12}^- (z_1^2 + z_3^2) + \eta_{12}^+ z_1 (1 - z_3^2)] \quad (36)$$

Now we are ready for the computation of the transmission  $T_s$  and reflection  $R_s$  probabilities. For this purpose, we introduce the associated current density  $J$ , which defines  $R_s$  and  $T_s$  as follows

$$T_s = \frac{J_{\text{tra}}}{J_{\text{inc}}}, \quad R_s = \frac{J_{\text{ref}}}{J_{\text{inc}}} \quad (37)$$

where  $J_{\text{inc}}$ ,  $J_{\text{ref}}$  and  $J_{\text{tra}}$  stand for the incident, reflected and transmitted components of the current density, respectively. It is easy to show

$$J = ev_F \Phi^\dagger \sigma_x \Phi \quad (38)$$

which gives rise to the following results

$$J_{\text{inc}} = ev_F (\Phi_1^+)^\dagger \sigma_x \Phi_1^+ \quad (39)$$

$$J_{\text{ref}} = ev_F (\Phi_1^-)^\dagger \sigma_x \Phi_1^- \quad (40)$$

$$J_{\text{tra}} = ev_F \Phi_5^\dagger \sigma_x \Phi_5 \quad (41)$$

and allow us to express the transmission and reflection probabilities as

$$T_s = |t_s|^2, \quad R_s = |r_s|^2. \quad (42)$$

We need to point out that we were able to consider a separate transmission probability for each of the propagating modes in the leads, because the matching condition does not mix these modes. Under such circumstances, physical measurable quantities such as conductance will be obtained using Landauer formula where summation of over all modes is performed.

### 3.3 Numerical results: electrostatic double barrier

The transmission  $T_s$  of Dirac electrons in graphene scattered by a triangular double barrier potential are evaluated numerically as a function of our system parameters: the energy  $\epsilon$ , the  $y$ -direction wave vector  $k_y$ , the energy gap  $\mu$ , the barriers widths  $(d_1, d_2)$ , the strength of potential barriers  $(v_1, v_2)$ .

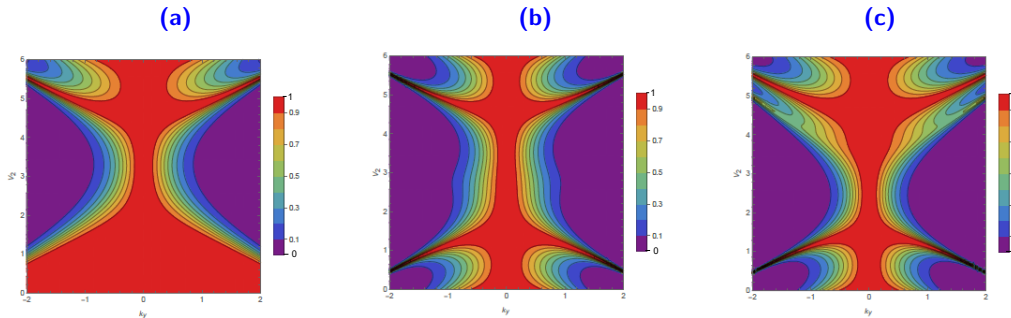


**Figure 2** – (color online) Contour plot for  $T(v_2, k_y)$  with the following parameters:  $d_1 = 1$ ,  $d_2 = 2$ ,  $\epsilon = 3$ ,  $\mu = 0$ . Let  $v_2$  changes from 0 to 6 and  $k_y$  from -2 to -0.001 and 0.001 to 2 that is to say  $k_y$  from -2 to 2 and  $k_y \neq 0$ . (a):  $v_1 = 0.5$ . (b):  $v_1 = 4$ . (c):  $v_1 = 8$ .

In Figure 2 we present the contour plot of the transmission probability  $T = tt^\dagger$  for a triangular double barrier structure as a function of well potential  $v_2$  and the transverse wave vector  $k_y$ . This has

been performed by fixing the parameters  $d_1 = 1$ ,  $d_2 = 2$ ,  $\epsilon = 3$ ,  $\mu = 0$  for three different values of the potential height  $v_1 = 0.5$ ,  $v_1 = 4$  and  $v_1 = 8$  corresponding to figures 2a, 2b and 2c, respectively. Note that the strength of the potential height  $v_1$  in this figure is proportional to the strength of the applied electrostatic field. The different colors from purple to red correspond to different values of the transmission continuously from 0 to 1. The number of oscillations increases as the strength of the electric field increases. The resonances that are clear in the transmission probability show up as peaks, we also observe the occurrence of a new strong and sharp resonance around  $v_2 = \epsilon$ .

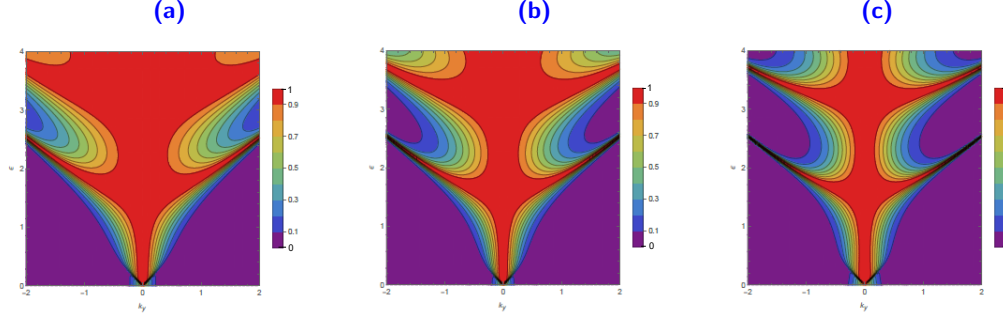


**Figure 3** – (color online) Contour plot for  $T(\epsilon, k_y)$  with the following parameters:  $d_1 = 1$ ,  $d_2 = 2$ ,  $\mu = 0$ ,  $v_2 = 0$ . Let  $\epsilon$  changes from 0 to 4 and  $k_y$  from -2 to -0.001 and then from 0.001 to 2 that is to say  $k_y$  from -2 to 2 and  $k_y \neq 0$ . (a):  $v_1 = 2$ . (b):  $v_1 = 3$ . (c):  $v_1 = 5$ .

In Figure 3 we show the contour plot of the transmission probability as function of energy  $\epsilon$  and the transfer wave vector  $k_y$  for  $d_1 = 1$ ,  $d_2 = 2$ , gapless graphene  $\mu = 0$  and three different values for potential  $v_1$ . Here, we take the case with  $v_1 = 2$  in figure 3a initially and then increase  $v_1$  from  $v_1 = 3$  in figure 3b to  $v_1 = 5$  in figure 3c and notice that the number of oscillations increases, when the incidence is almost normal, the wave vector is close to  $k_y \approx 0$  associated with total transmission. We see that full transmission is squeezed into a very narrow angle region around normal incidence,  $k_y \approx 0$ , when we increase the strength of the electrostatic field make it favorable application to tunneling collimation.

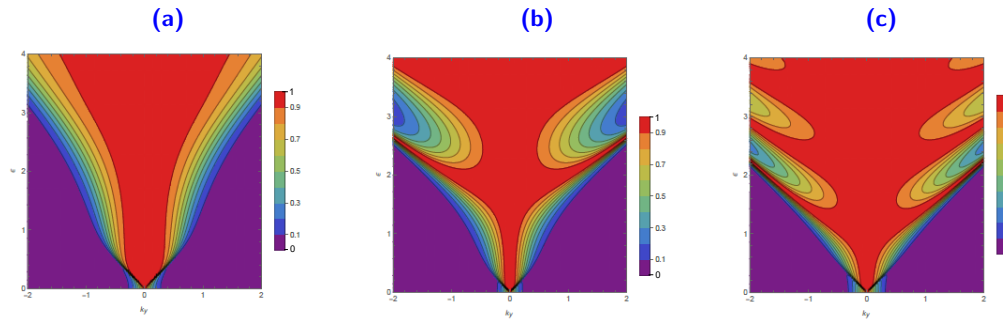
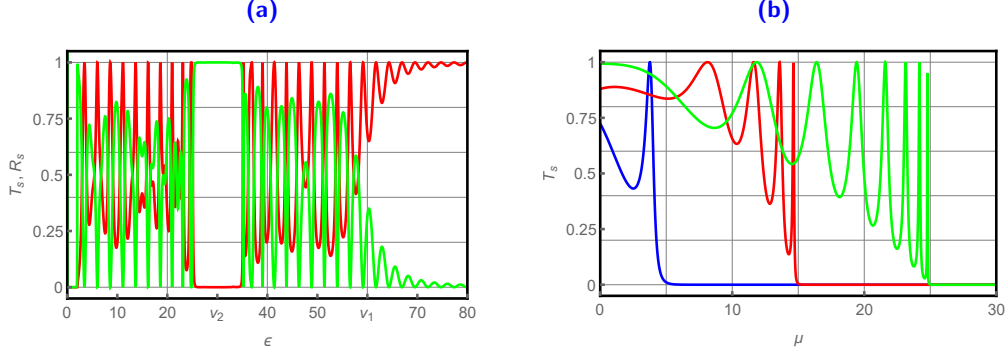


**Figure 4** – (color online) Contour plot for  $T(\epsilon, k_y)$  with the following parameters:  $v_1 = 2$ ,  $d_2 = 2$ ,  $\mu = 0$ ,  $v_2 = 0$ . Let  $\epsilon$  changes from 0 to 4 and  $k_y$  from -2 to -0.001 and then from 0.001 to 2 that is to say  $k_y$  from -2 to 2 and  $k_y \neq 0$ . (a):  $d_1 = 0.1$ . (b):  $d_1 = 0.9$ . (c):  $d_1 = 1.5$ .

In Figure 4 we show the contour plot of the transmission probability as function of energy  $\epsilon$  and the transverse wave vector  $k_y$  from -2 to 2 and  $k_y \neq 0$ , we fix the potential  $v_1 = 2$ ,  $v_2 = 0$ , the barrier width  $d_2 = 2$ , for gapless graphene  $\mu = 0$  and three different values of the barrier width  $d_1 = 0.1$  in

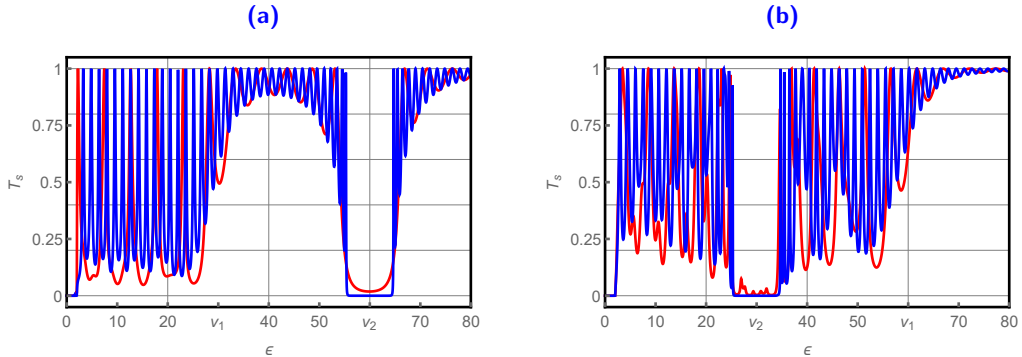


figure 4a,  $d_1 = 0.0.9$  in figure 4b and  $d_1 = 1.5$  in figure 4c. By increasing the width  $d_1$  the number of oscillation peaks increases. The parameters of the triangular potential ( $v_1, d_2 - d_1$ ), whose ratio represents the strength of the applied electrostatic field, are found to play a key role in controlling the tunneling resistance peak. All these predicted attractive transport properties are expected to be extremely useful for designing both novel electronic and optical graphene-based devices and electronic lenses in ballistic-electron optics.



**Figure 5** – (color online) (a): Transmission (red color) and reflection (green color) probabilities ( $T_s, R_s$ ) as a function of energy  $\epsilon$  with  $d_1 = 0.6$ ,  $d_2 = 2.5$ ,  $\mu = 4$ ,  $k_y = 2$ ,  $v_1 = 60$  and  $v_2 = 30$ . (b): Transmission probability  $T_s$  as a function of energy gap  $\mu$  with  $d_1 = 0.5$ ,  $d_2 = 1.5$ ,  $k_y = 1$ ,  $v_1 = 50$ ,  $v_2 = 40$ ,  $\epsilon = 15$  (green color),  $\epsilon = 25$  (red color) and  $\epsilon = 35$  (blue color).

In Figure 5a we show the transmission and reflection probabilities versus the energy  $\epsilon$ . Obviously, we can check that the probability conservation condition  $T_s + R_s = 1$  is well satisfied. In the first energy interval  $\epsilon \leq k_y$  we have no transmission because it is a forbidden zone. However, in the second energy intervals  $k_y \leq \epsilon \leq v_2 - k_y - \frac{\mu}{2}$  and  $v_2 + k_y + \frac{\mu}{2} \leq \epsilon \leq v_1$ , we observe resonance oscillations due to the Klein regime. We have no transmission (gap region) when  $v_2 - k_y - \frac{\mu}{2} \leq \epsilon \leq v_2 + k_y + \frac{\mu}{2}$ . Finally, in the interval where  $\epsilon > v_1$ , there exist usual high energy oscillations, which saturate asymptotically. Note that (13) implies that for certain energy gap  $\mu$ , there is no transmission. In fact, under the condition  $\mu > |v_2 - \epsilon|$  every incoming wave is reflected. In Figure 5b we see that the transmission vanishes for values of  $\epsilon$  below the critical value  $\mu = |v_2 - \epsilon|$ .



**Figure 6** – (color online) Transmission probability for the static barrier  $T_s$  as a function of energy  $\epsilon$  with  $d_1 = 0.3$  (red color),  $d_1 = 1$  (blue color),  $d_2 = 2.5$ ,  $\mu = 4$  and  $k_y = 2$ . (a): for  $v_1 \leq v_2$ :  $v_1 = 30$ ,  $v_2 = 60$ . (b): for  $v_1 \geq v_2$ :  $v_1 = 60$ ,  $v_2 = 30$ .

Figure 6 shows the transmission  $T_s$  as a function of incident electron energy  $\epsilon$  for the Dirac fermion scattered by a double triangular barriers with  $d_2 = 2.5$ ,  $\mu = 4$ ,  $k_y = 2$  and two values of barrier width  $d_1 = \{0.3, 1\}$ . In Figure 6a we consider the parameters  $v_1 = \frac{v_2}{2} = 30$  for the Dirac fermion scattered by a double barrier triangular potential where we distinguish five different zones. Indeed, the first is a forbidden zone where  $0 \leq \epsilon \leq k_y$ . The second zone  $k_y \leq \epsilon \leq v_1$  is the lower Klein energy zone with transmission resonances. The third zone contains transmission oscillations. The fourth one  $v_2 - k_y - \frac{\mu}{2} \leq \epsilon \leq v_2 + k_y + \frac{\mu}{2}$  is a window where the transmission is zero, the wavefunction is damped and transmission decays exponentially. The fifth zone  $\epsilon \geq v_2 + k_y + \frac{\mu}{2}$  contains over barrier oscillations, the transmission converges to unity at high energies similarly to the non-relativistic result. We also notice from Figure 6a that resonances move to the right as we increase the width of the field region (reduction of the electrostatic field). In Figure 6b we consider the opposite situation, that is  $v_1 = 2v_2 = 60$ , the results show that as long as the well width  $d_1$  increases the transmission resonances shift to the left and the width of the resonances increase in regions  $k_y \leq \epsilon \leq v_2 - k_y - \frac{\mu}{2}$  and  $v_2 + k_y + \frac{\mu}{2} \leq \epsilon \leq v_1$ .

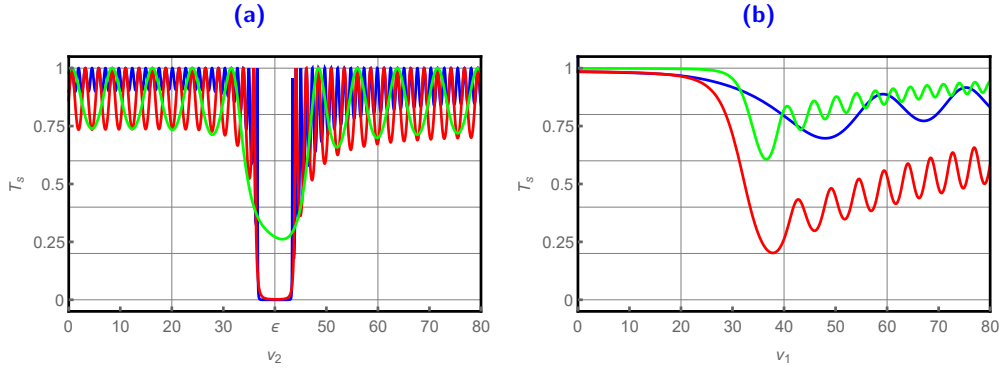


**Figure 7** – (color online) (a): Transmission probability through the static barrier  $T_s$  as a function of the potential  $v_2$  for  $d_1 = 0.2$  (green color),  $d_1 = 0.6$  (red color),  $d_1 = 1.2$  (blue color),  $d_2 = 2$ ,  $\mu = 3$ ,  $k_y = 1$ ,  $\epsilon = 40$  and  $v_1 = 60$ . (b): Transmission probability through the static barrier  $T_s$  as a function of the potential  $v_1$  with  $d_1 = 0.05$  (green color),  $d_1 = 0.7$  (red color),  $d_1 = 2$  (blue color),  $d_2 = 2.5$ ,  $\mu = 4$ ,  $k_y = 2$ ,  $\epsilon = 30$  and  $v_2 = 60$ .

We present in Figure 7a the transmission versus the potential  $v_2$ . It is clear that the two transmission curves are almost symmetric with respect to the point  $v_2 = \epsilon$ . While an increase in the value  $d_1$  widens the bowl width. As we increase the well width we see an increase in the number of resonances while a zero transmission region appears only for small values of  $d_1$  (large values of the electrostatic field). Figure 7b shows the transmission probability for a static barrier  $T_s$  as function of the strength of the applied voltage  $v_1$  for different widths of the electric field region. Full transmission is observed for small values of  $v_1$ , less than the energy of the incident fermion. It then decreases sharply for  $v_1 > \epsilon - (2k_y + \mu)$  until it reaches a relative minimum and then begins to increase in an oscillatory manner. However, we noticed that a gap region appeared for energies around the value of the elevated well potential,  $v_2 - k_y - \frac{\mu}{2} \leq \epsilon \leq v_2 + k_y + \frac{\mu}{2}$ , independently of the ordering strength of the potentials  $v_1$  and  $v_2$ . As a results, we observe that the double barrier strongly affect the transmission and then it can be used a tunable parameter to control the tunneling in our system, which can be used in technological applications.

## 4 Magnetic double barrier

Consider a two-dimensional system of Dirac fermions forming a graphene sheet. This sheet is subject to a double barrier potential in addition to a mass term and an externally applied magnetic field. Particles and antiparticles moving in the positive and negative energy regions, respectively, have a conserved component of the wave vector along the  $y$ -direction (mode) due to the fact that each of the  $N$  propagating modes in the leads is independent because the matching condition does not mix these modes. A uniform perpendicular magnetic field is applied, along the  $z$ -direction and confined to the well region between the two electrostatic barriers. It is defined by

$$B(x, y) = B\Theta(d_1^2 - x^2) \quad (43)$$

where  $B$  is the strength of the magnetic field within the strip located in the region  $|x| < d_1$  and  $B = 0$  otherwise,  $\Theta$  is the Heaviside unit step function. Choosing the Landau gauge and imposing continuity of the vector potential at the boundary to avoid unphysical effects, we end up with the following vector potential

$$A_y(x) = A_j = \frac{c}{e} \times \begin{cases} -\frac{1}{l_B^2}d_1, & x < -d_2 \\ \frac{1}{l_B^2}x, & |x| < d_1 \\ \frac{1}{l_B^2}d_1, & x \geq d_2 \end{cases} \quad (44)$$

with the magnetic field length  $l_B = \sqrt{1/B}$  in the unit system ( $\hbar = c = e = 1$ ). The system is composed of five regions denoted  $j = 1, 2, 3, 4, 5$ . The left region ( $j = 1$ ) describes the incident electron beam with energy  $E = v_F\epsilon$  at an incident angle  $\phi_1$  where  $v_F$  is the Fermi velocity. The extreme right region ( $j = 5$ ) describes the transmitted electron beam at an angle  $\phi_5$ . The Hamiltonian for describing our system reads as

$$H_m = v_F \boldsymbol{\sigma} \cdot \left( \mathbf{p} + \frac{e}{c} \mathbf{A} \right) + V(x)\mathbb{I}_2 + G_p\Theta(d_1^2 - x^2)\sigma_z. \quad (45)$$

To proceed further, we need to find the solutions of the corresponding Dirac equation and their associated energy spectrum.

### 4.1 Energy spectrum: presence of magnetic field

We are set to determine the eigenvalues and eigenspinors of the Hamiltonian  $H_m$ . Indeed, the Dirac Hamiltonian describing regions 1 and 5, is obtained from (45) as

$$H_m = \begin{pmatrix} 0 & v_F(p_{xj} - i(p_y + \frac{e}{c}A_j)) \\ v_F(p_{xj} + i(p_y + \frac{e}{c}A_j)) & 0 \end{pmatrix}. \quad (46)$$

The corresponding time independent Dirac equation for the spinor  $\psi_j(x, y) = (\varphi_j^+, \varphi_j^-)^T$  at energy  $E = v_F\epsilon$  is given by

$$H_m \begin{pmatrix} \varphi_j^+ \\ \varphi_j^- \end{pmatrix} = \epsilon \begin{pmatrix} \varphi_j^+ \\ \varphi_j^- \end{pmatrix}. \quad (47)$$

This eigenvalue problem can be written as two linear differential equations of the form

$$p_{xj} - i\left(p_y + \frac{e}{c}A_j\right)\varphi_j^- = \epsilon\varphi_j^+ \quad (48)$$

$$p_{xj} + i\left(p_y + \frac{e}{c}A_j\right)\varphi_j^+ = \epsilon\varphi_j^- \quad (49)$$

which gives the energy eigenvalue

$$\epsilon = s_j \sqrt{p_{xj}^2 + \left(p_y + \frac{e}{c} A_j\right)^2} \quad (50)$$

where  $s_j = \text{sgn}(\epsilon)$ , the incoming momentum  $\mathbf{p}_j = (p_{xj}, p_y)$  and position  $\mathbf{r} = (x, y)$ . The incoming spinor is

$$\psi_{in} = \frac{1}{\sqrt{2}} \begin{pmatrix} 1 \\ z_{p_{xj}} \end{pmatrix} e^{i\mathbf{p}_j \cdot \mathbf{r}}, \quad z_{p_{xj}} = z_j = s_j e^{i\phi_j} \quad (51)$$

with  $s_0 = \text{sgn}(\epsilon)$  and  $\phi_j = \arctan\left(\frac{p_y - \frac{e}{c} A_j}{p_{xj}}\right)$  is the angle that the incident electron beam makes with the  $x$ -direction,  $p_{x1}$  and  $p_y$  are the  $x$  and  $y$ -components of the electron wave vector, respectively. The eigenspinors are given by

$$\psi_j^+ = \frac{1}{\sqrt{2}} \begin{pmatrix} 1 \\ z_j \end{pmatrix} e^{i(p_{xj}x + p_y y)} \quad (52)$$

$$\psi_j^- = \frac{1}{\sqrt{2}} \begin{pmatrix} 1 \\ -z_j^* \end{pmatrix} e^{i(-p_{xj}x + p_y y)}. \quad (53)$$

It is straightforward to solve the tunneling problem for Dirac fermions. We assume that the incident wave propagates at the angle  $\phi_1$  with respect to the  $x$ -direction and write the components, of the Dirac spinor  $\varphi_j^+$  and  $\varphi_j^-$ , for each region. For  $x < -d_2$  (region 1):

$$\epsilon = \left[ p_{x1}^2 + \left( p_y - \frac{1}{l_B^2} d_1 \right)^2 \right]^{\frac{1}{2}} \quad (54)$$

$$\psi_1 = \frac{1}{\sqrt{2}} \begin{pmatrix} 1 \\ z_1 \end{pmatrix} e^{i(p_{x1}x + p_y y)} + r_m \frac{1}{\sqrt{2}} \begin{pmatrix} 1 \\ -z_1^* \end{pmatrix} e^{i(-p_{x1}x + p_y y)} \quad (55)$$

$$z_1 = s_1 \frac{p_{x1} + i \left[ p_y - \frac{1}{l_B^2} d_1 \right]}{\sqrt{p_{x1}^2 + \left[ p_y - \frac{1}{l_B^2} d_1 \right]^2}}. \quad (56)$$

In the barrier  $x > d_2$  (region 5):

$$\epsilon = \left[ p_{x5}^2 + \left( p_y + \frac{1}{l_B^2} d_1 \right)^2 \right]^{\frac{1}{2}} \quad (57)$$

$$\psi_5 = \frac{1}{\sqrt{2}} t_m \begin{pmatrix} 1 \\ z_5 \end{pmatrix} e^{i(p_{x5}x + p_y y)} \quad (58)$$

$$z_5 = s_5 \frac{p_{x5} + i \left[ p_y + \frac{1}{l_B^2} d_1 \right]}{\sqrt{p_{x5}^2 + \left[ p_y + \frac{1}{l_B^2} d_1 \right]^2}}. \quad (59)$$

In region 2 and 4 ( $d_1 < |x| < d_2$ ): The general solution can be expressed in terms of the parabolic cylinder function [11, 17, 18] as

$$\chi_\gamma^+ = c_1 D_{\nu_\gamma - 1}(Q_\gamma) + c_2 D_{-\nu_\gamma}(-Q_\gamma^*) \quad (60)$$

where  $\nu_\gamma = \frac{i}{2\varrho} \left( k_y - \gamma \frac{d_1}{l_B^2} \right)^2$ ,  $\epsilon_0 = \epsilon - v_1$  and  $Q_\gamma(x) = \sqrt{\frac{2}{\varrho}} e^{i\pi/4} (\gamma \varrho x + \epsilon_0)$ ,  $c_1$  and  $c_2$  are constants. It gives the other component

$$\begin{aligned} \chi_\gamma^- &= -c_2 \frac{1}{k_y - \gamma \frac{d_1}{l_B^2}} \left[ 2(\epsilon_0 + \gamma \varrho x) D_{-\nu_\gamma} (-Q_\gamma^*) + \sqrt{2\varrho} e^{i\pi/4} D_{-\nu_\gamma+1} (-Q_\gamma^*) \right] \\ &\quad - \frac{c_1}{k_y - \gamma \frac{d_1}{l_B^2}} \sqrt{2\varrho} e^{-i\pi/4} D_{\nu_\gamma-1} (Q_\gamma). \end{aligned} \quad (61)$$

The components of the spinor solution of the Dirac equation (3) in region 2 and 4 can be obtained from (60) and (61) with  $\varphi_\gamma^+(x) = \chi_\gamma^+ + i\chi_\gamma^-$  and  $\varphi_\gamma^-(x) = \chi_\gamma^+ - i\chi_\gamma^-$ . We have the eigenspinor

$$\psi_j = a_{j-1} \begin{pmatrix} u_\gamma^+(x) \\ u_\gamma^-(x) \end{pmatrix} e^{ik_y y} + a_j \begin{pmatrix} v_\gamma^+(x) \\ v_\gamma^-(x) \end{pmatrix} e^{ik_y y} \quad (62)$$

where  $j = 2, 4$  and  $\gamma = \pm 1$ , the function  $u_\gamma^\pm(x)$  and  $v_\gamma^\pm(x)$  are given by

$$u_\gamma^\pm(x) = D_{\nu_\gamma-1}(Q_\gamma) \mp \frac{1}{k_y - \gamma \frac{d_1}{l_B^2}} \sqrt{2\varrho} e^{i\pi/4} D_{\nu_\gamma}(Q_\gamma) \quad (63)$$

$$\begin{aligned} v_\gamma^\pm(x) &= \pm \frac{1}{k_y - \gamma \frac{d_1}{l_B^2}} \sqrt{2\varrho} e^{-i\pi/4} D_{-\nu_\gamma+1} (-Q_\gamma^*) \\ &\quad \pm \frac{1}{k_y - \gamma \frac{d_1}{l_B^2}} \left( -2i\epsilon_0 \pm \left( k_y - \gamma \frac{d_1}{l_B^2} \right) - \gamma 2i\varrho x \right) D_{-\nu_\gamma} (-Q_\gamma^*). \end{aligned} \quad (64)$$

In region 2:

$$\psi_2 = a_1 \begin{pmatrix} u_1^+(x) \\ u_1^-(x) \end{pmatrix} e^{ik_y y} + a_2 \begin{pmatrix} v_1^+(x) \\ v_1^-(x) \end{pmatrix} e^{ik_y y} \quad (65)$$

In region 4:

$$\psi_4 = a_3 \begin{pmatrix} u_{-1}^+(x) \\ u_{-1}^-(x) \end{pmatrix} e^{ik_y y} + a_4 \begin{pmatrix} v_{-1}^+(x) \\ v_{-1}^-(x) \end{pmatrix} e^{ik_y y} \quad (66)$$

In the region  $|x| \leq d_1$ : From the nature of the system under consideration, we write the Hamiltonian corresponding to region 3 in matrix form as

$$H_m = v_F \begin{pmatrix} \frac{V_2}{v_F} + \frac{G_p}{v_F} & -i \frac{\sqrt{2}}{l_B} \left( \frac{l_B}{\sqrt{2}} (\partial_x - i\partial_y + \frac{e}{c} A_3) \right) \\ i \frac{\sqrt{2}}{l_B} \left( \frac{l_B}{\sqrt{2}} (-\partial_x - i\partial_y + \frac{e}{c} A_3) \right) & \frac{V_2}{v_F} - \frac{G_p}{v_F} \end{pmatrix} \quad (67)$$

Note that, the energy gap  $G_p$  behaves like a mass term in Dirac equation. Certainly this will affect the above results and leads to interesting consequences on the transport properties of our system. We determine the eigenvalues and eigenspinors of the Hamiltonian  $H_m$  by considering the time independent equation for the spinor  $\psi_3(x, y) = (\psi_3^+, \psi_3^-)^T$  using the fact that the transverse momentum  $p_y$  is conserved, we can write the wave function  $\psi_3(x, y) = e^{ip_y y} \varphi_3(x)$  with  $\varphi_3(x) = (\varphi_3^+, \varphi_3^-)^T$ , the energy being defined by  $E = v_F \epsilon$  leads to

$$H_m \begin{pmatrix} \varphi_3^+ \\ \varphi_3^- \end{pmatrix} = \epsilon \begin{pmatrix} \varphi_3^+ \\ \varphi_3^- \end{pmatrix} \quad (68)$$

At this stage, it is convenient to introduce the annihilation and creation operators. They can be defined as

$$a = \frac{l_B}{\sqrt{2}} \left( \partial_x + k_y + \frac{e}{c} A_3 \right), \quad a^\dagger = \frac{l_B}{\sqrt{2}} \left( -\partial_x + k_y + \frac{e}{c} A_3 \right) \quad (69)$$

which obey the canonical commutation relations  $[a, a^\dagger] = \mathbb{I}$ . Rescaling our energies  $G_p = v_F \mu$  and  $V_2 = v_F v_2$ , (68) can be written in terms of  $a$  and  $a^\dagger$  as

$$\begin{pmatrix} v_2 + \mu & -i\frac{\sqrt{2}}{l_B} a \\ +i\frac{\sqrt{2}}{l_B} a^\dagger & v_2 - \mu \end{pmatrix} \begin{pmatrix} \varphi_3^+ \\ \varphi_3^- \end{pmatrix} = \epsilon \begin{pmatrix} \varphi_3^+ \\ \varphi_3^- \end{pmatrix} \quad (70)$$

which gives

$$(v_2 + \mu)\varphi_3^+ - i\frac{\sqrt{2}}{l_B} a\varphi_3^- = \epsilon\varphi_3^+ \quad (71)$$

$$i\frac{\sqrt{2}}{l_B} a^\dagger\varphi_3^+ + (v_2 - \mu)\varphi_3^- = \epsilon\varphi_3^-. \quad (72)$$

Injecting (72) in (71), we obtain a differential equation of second order for  $\varphi_3^+$

$$[(\epsilon - v_2)^2 - \mu^2] \varphi_3^+ = \frac{2}{l_B^2} a a^\dagger \varphi_3^+. \quad (73)$$

It is clear that  $\varphi_3^+$  is an eigenstate of the number operator  $\hat{N} = a^\dagger a$  and therefore we identify  $\varphi_3^+$  with the eigenstates of the harmonic oscillator  $|n-1\rangle$ , namely

$$\varphi_3^+ \sim |n-1\rangle \quad (74)$$

which gives for (85)

$$[(\epsilon - v_2)^2 - \mu^2] |n-1\rangle = \frac{2}{l_B^2} n |n-1\rangle \quad (75)$$

and the associated energy spectrum is

$$\epsilon - v_2 = s_3 \epsilon_n = s_3 \frac{1}{l_B} \sqrt{(\mu l_B)^2 + 2n} \quad (76)$$

where we have set  $\epsilon_n = s_3(\epsilon - v_2)$  and  $s_3 = \text{sign}(\epsilon_n - v_2)$  correspond to positive and negative energy solutions. For this reason we write the eigenvalues as

$$\epsilon = v_2 + s_3 \frac{1}{l_B} \sqrt{(\mu l_B)^2 + 2n} \quad (77)$$

The second eigenspinor component then can be obtained from

$$\varphi_3^- = \frac{i\sqrt{2}a^\dagger}{(\epsilon - v_2)l_B + \mu l_B} |n-1\rangle = \frac{i\sqrt{2n}}{(\epsilon - v_2)l_B + \mu l_B} |n\rangle \quad (78)$$

where  $\sqrt{2n} = \sqrt{(\epsilon_n l_B)^2 - (\mu l_B)^2}$ . We find

$$\varphi_3^- = s_3 i \sqrt{\frac{\epsilon_n l_B - s_3 \mu l_B}{\epsilon_n l_B + s_3 \mu l_B}} |n\rangle \quad (79)$$

After normalization we arrive at the following expression for the positive and negative energy eigenstates

$$\varphi_3 = \frac{1}{\sqrt{2}} \begin{pmatrix} \sqrt{\frac{\epsilon_n l_B + s_3 \mu l_B}{\epsilon_n l_B}} |n-1\rangle \\ s_3 i \sqrt{\frac{\epsilon_n l_B - s_3 \mu l_B}{\epsilon_n l_B}} |n\rangle \end{pmatrix} \quad (80)$$

Introducing the parabolic cylinder functions  $D_n(x) = 2^{-\frac{n}{2}} e^{-\frac{x^2}{4}} H_n\left(\frac{x}{\sqrt{2}}\right)$ , we express the solution in region 3 as

$$\psi_3(x, y) = b_1 \psi_3^+ + b_2 \psi_3^- \quad (81)$$

with its two components

$$\psi_3^\pm(x, y) = \frac{1}{\sqrt{2}} \begin{pmatrix} \sqrt{\frac{\epsilon_n l_B + s_3 \mu l_B}{\epsilon_n l_B}} D_{((\epsilon_n l_B)^2 - (\mu l_B)^2)/2-1} \left( \pm \sqrt{2} \left( \frac{x}{l_B} + k_y l_B \right) \right) \\ \pm i \frac{s_3 \sqrt{2}}{\sqrt{\epsilon_n l_B (\epsilon_n l_B + s_3 \mu l_B)}} D_{((\epsilon_n l_B)^2 - (\mu l_B)^2)/2} \left( \pm \sqrt{2} \left( \frac{x}{l_B} + k_y l_B \right) \right) \end{pmatrix} e^{ik_y y} \quad (82)$$

As usual the coefficients  $(a_1, a_2, a_3, a_4, b_1, b_2, r, t)$  can be determined using the boundary conditions, continuity of the eigenspinors at each interface.

## 4.2 Transmission and reflection: presence of magnetic field

We will now study some interesting features of our system which are reflected in the corresponding transmission probability. Before doing so, let us simplify our writing using the following shorthand notation

$$\vartheta_{\tau 1}^\pm = D_{[(\epsilon_n l_B)^2 - (\mu l_B)^2]/2-1} \left[ \pm \sqrt{2} \left( \frac{\tau d_1}{l_B} + k_y l_B \right) \right] \quad (83)$$

$$\zeta_{\tau 1}^\pm = D_{[(\epsilon_n l_B)^2 - (\mu l_B)^2]/2} \left[ \pm \sqrt{2} \left( \frac{\tau d_1}{l_B} + k_y l_B \right) \right] \quad (84)$$

$$f_1^\pm = \sqrt{\frac{\epsilon_n \pm \mu}{\epsilon_n}}, \quad f_2^\pm = \frac{\sqrt{2/l_B^2}}{\sqrt{\epsilon_n (\epsilon_n \pm \mu)}} \quad (85)$$

$$u_\gamma^\pm(\tau d_1) = u_{\gamma, \tau 1}^\pm, \quad u_\gamma^\pm(\tau d_2) = u_{\gamma, \tau 2}^\pm \quad (86)$$

$$v_\gamma^\pm(\tau d_1) = v_{\gamma, \tau 1}^\pm, \quad v_\gamma^\pm(\tau d_2) = v_{\gamma, \tau 2}^\pm \quad (87)$$

where  $\tau = \pm$ . Dirac equation requires the following set of continuity conditions

$$\psi_1(-d_2) = \psi_2(-d_2), \quad \psi_2(-d_1) = \psi_3(-d_1), \quad \psi_3(d_1) = \psi_4(d_1), \quad \psi_4(d_2) = \psi_5(d_2) \quad (88)$$

That is, requirement of the continuity of the spinor wave functions at each junction interface gives rise to the above set of equations. We prefer to express these relationships in terms of  $2 \times 2$  transfer matrices between  $j$ -th and  $(j+1)$ -th regions,  $\mathcal{M}_{j,j+1}$ , we obtain the full transfer matrix over the whole double barrier which can be written, in an obvious notation, as follows

$$\begin{pmatrix} 1 \\ r_m \end{pmatrix} = \prod_{j=1}^4 \mathcal{M}_{j,j+1} \begin{pmatrix} t_m \\ 0 \end{pmatrix} = \mathcal{M} \begin{pmatrix} t_m \\ 0 \end{pmatrix} \quad (89)$$

where the total transfer matrix  $\mathcal{M} = \mathcal{M}_{12} \cdot \mathcal{M}_{23} \cdot \mathcal{M}_{34} \cdot \mathcal{M}_{45}$  are transfer matrices that couple the wave function in the  $j$ -th region to the wave function in the  $(j+1)$ -th region. These are given explicitly

by the forms

$$\mathcal{M} = \begin{pmatrix} \tilde{m}_{11} & \tilde{m}_{12} \\ \tilde{m}_{21} & \tilde{m}_{22} \end{pmatrix} \quad (90)$$

$$\mathcal{M}_{12} = \begin{pmatrix} e^{-ip_{x1}d_2} & e^{ip_{x1}d_2} \\ z_1 e^{-ip_{x1}d_2} & -z_1^* e^{ip_{x1}d_2} \end{pmatrix}^{-1} \begin{pmatrix} u_{1,-2}^+ & v_{1,-2}^+ \\ u_{1,-2}^- & v_{1,-2}^- \end{pmatrix} \quad (91)$$

$$\mathcal{M}_{23} = \begin{pmatrix} u_{1,-1}^+ & v_{1,-1}^+ \\ u_{1,-1}^- & v_{1,-1}^- \end{pmatrix}^{-1} \begin{pmatrix} \vartheta_1^+ & \vartheta_1^- \\ \zeta_1^+ & \zeta_1^- \end{pmatrix} \quad (92)$$

$$\mathcal{M}_{34} = \begin{pmatrix} \vartheta_{-1}^+ & \vartheta_{-1}^- \\ \zeta_{-1}^+ & \zeta_{-1}^- \end{pmatrix}^{-1} \begin{pmatrix} u_{-1,1}^+ & v_{-1,1}^+ \\ u_{-1,1}^- & v_{-1,1}^- \end{pmatrix} \quad (93)$$

$$\mathcal{M}_{45} = \begin{pmatrix} u_{-1,2}^+ & v_{-1,2}^+ \\ u_{-1,2}^- & v_{-1,2}^- \end{pmatrix}^{-1} \begin{pmatrix} e^{ip_{x5}d_2} & e^{-ip_{x5}d_2} \\ z_5 e^{ip_{x5}d_2} & -z_5^* e^{-ip_{x5}d_2} \end{pmatrix}. \quad (94)$$

These will enable us to compute the reflection and transmission amplitudes

$$t_m = \frac{1}{\tilde{m}_{11}}, \quad r_m = \frac{\tilde{m}_{21}}{\tilde{m}_{11}}. \quad (95)$$

More explicitly, we have for transmission

$$t_m = \frac{e^{id_2(p_{x1}+p_{x5})} (1+z_5^2) (\vartheta_1^- \zeta_1^+ + \vartheta_1^+ \zeta_1^-)}{f_2^+ (f_1^- \mathcal{L}_1 + i f_2^- \mathcal{L}_2) + f_1^+ (f_2^- \mathcal{L}_3 + i f_1^- \mathcal{L}_4)} \mathcal{D} \quad (96)$$

where the quantities  $\mathcal{D}$ ,  $\mathcal{L}_1$ ,  $\mathcal{L}_2$ ,  $\mathcal{L}_3$  and  $\mathcal{L}_4$  are defined by

$$\mathcal{D} = \left( u_{-1,1}^- v_{-1,1}^+ - u_{-1,1}^+ v_{-1,1}^- \right) \left( u_{1,-2}^+ v_{1,-2}^- - u_{1,-2}^- v_{1,-2}^+ \right) \quad (97)$$

$$\mathcal{L}_1 = \vartheta_{-1}^- \zeta_1^+ \mathcal{F} \mathcal{G} - \vartheta_{-1}^+ \zeta_1^- \mathcal{K} \mathcal{J} \quad (98)$$

$$\mathcal{L}_2 = (\zeta_1^+ \zeta_{-1}^- - \zeta_1^- \zeta_{-1}^+) \mathcal{F} \mathcal{J} \quad (99)$$

$$\mathcal{L}_3 = \vartheta_{-1}^+ \zeta_1^- \mathcal{F} \mathcal{G} - \vartheta_{-1}^- \zeta_1^+ \mathcal{K} \mathcal{J} \quad (100)$$

$$\mathcal{L}_4 = (\vartheta_1^+ \vartheta_{-1}^- - \vartheta_1^- \vartheta_{-1}^+) \mathcal{K} \mathcal{G} \quad (101)$$

and

$$\mathcal{F} = \left[ u_{1,-1}^+ v_{1,-2}^- - u_{1,-2}^+ v_{1,-1}^- - z_1 \left( u_{1,-1}^+ v_{1,-2}^+ - u_{1,-2}^+ v_{1,-1}^+ \right) \right] \quad (102)$$

$$\mathcal{G} = \left[ u_{-1,1}^- v_{-1,2}^+ - u_{-1,2}^- v_{-1,1}^+ + z_5 \left( u_{-1,1}^- v_{-1,2}^- - u_{-1,2}^- v_{-1,1}^- \right) \right] \quad (103)$$

$$\mathcal{K} = \left[ u_{1,-1}^- v_{1,-2}^- - u_{1,-2}^- v_{1,-1}^- - z_1 \left( u_{1,-1}^- v_{1,-2}^+ - u_{1,-2}^- v_{1,-1}^+ \right) \right] \quad (104)$$

$$\mathcal{J} = \left[ u_{-1,1}^+ v_{-1,2}^+ - u_{-1,2}^+ v_{-1,1}^+ + z_5 \left( u_{-1,1}^+ v_{-1,2}^- - u_{-1,2}^+ v_{-1,1}^- \right) \right] \quad (105)$$

Actually the transmission probabilities  $T_m$  and reflection  $R_m$  for each independent mode can be obtained using the corresponding electric current density  $J$  for our system. From our previous Hamiltonian, we can show that incident, reflected and transmitted currents take the following forms

$$J_{\text{inc},m} = ev_F (\psi_1^+)^\dagger \sigma_x \psi_1^+ \quad (106)$$

$$J_{\text{ref},m} = ev_F (\psi_1^-)^\dagger \sigma_x \psi_1^- \quad (107)$$

$$J_{\text{tra},m} = ev_F \psi_5^\dagger \sigma_x \psi_5. \quad (108)$$



These can be used to write the reflection and transmission probabilities as

$$T_m = \frac{p_{x5}}{p_{x1}} |t_m|^2, \quad R_m = |r_m|^2. \quad (109)$$

### 4.3 Numerical results: presence of magnetic field

The physical outcome of particle scattering through the double triangular barrier depends on the energy of the incoming particle. We numerically evaluate the transmission probability  $T_m$  as a function of structural parameters of the graphene triangular double barrier in the presence of a perpendicular magnetic field, in terms of the energy  $\epsilon$ , the  $y$ -component of the wave vector  $k_y$ , the magnetic field  $B$ , the energy gap  $\mu$  and the applied potentials  $v_1$  and  $v_2$ . The results are shown in Figures 8, 9 and 10. In addition to the expected above-barrier full transmission for some values of  $\epsilon l_B$  and  $v_2 l_B$ . We note that in Figure 8a, when the energy is less than the height of the potential barrier  $\epsilon l_B < k_y l_B + \frac{d_1}{l_B}$ , we have zero transmission. In the second interval  $k_y l_B + \frac{d_1}{l_B} \leq \epsilon l_B \leq v_1 l_B$  the third zone contains oscillations. Finally the interval  $\epsilon l_B > v_1 l_B$  contains the usual over barrier oscillations and asymptotically goes to unity at high energy. Figure 8b shows the transmission spectrum for different transverse wave vector  $k_y l_B$ , the energy gap  $\mu l_B$  is zero and  $v_2 l_B = 0$ . We see that if we increase the wave vector  $k_y l_B$  the zone of zero transmission increases according to the condition  $\epsilon l_B < k_y l_B + \frac{d_1}{l_B}$ . In the second interval the transmission oscillates get very close to sharp Fabry–Pérot type of resonances and zero transmission regions appear as  $k_y l_B$  increases. Finally in the interval  $\epsilon l_B > v_1 l_B$  the transmission increases to its asymptotic value.

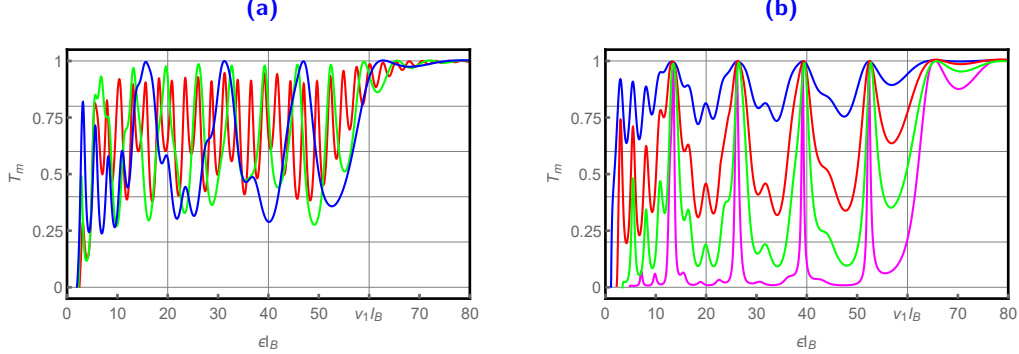


**Figure 8** – (color online) Transmission probability  $T_m$  for the magnetic barrier as a function of energy  $\epsilon l_B$  with  $\frac{d_2}{l_B} = 1.5$ ,  $v_1 l_B = 60$ ,  $v_2 l_B = 0$  and  $\mu l_B = 0$ . (a) for  $k_y l_B = 2$ ,  $\frac{d_1}{l_B} = 0.12$  (blue color),  $\frac{d_1}{l_B} = 0.24$  (green color) and  $\frac{d_1}{l_B} = 0.6$  (red color). (b) for  $\frac{d_1}{l_B} = 0.12$ ,  $k_y l_B = 1$  (blue color),  $k_y l_B = 2$  (red color),  $k_y l_B = 3$  (green color) and  $k_y l_B = 5$  (magenta color).

On the other hand, if we keep the same well region and cancel both the applied magnetic field and mass term in the well region, the series of potentials behave like a simple double barrier with the same effective mass  $k_y$ . Thus, in this case we reproduce exactly the transmission obtained in [?], for the massive Dirac equation with  $m = k_y$ . Let us treat the triangular double barrier case when  $v_2 < v_1$  and  $v_2 > v_1$ . In both cases, the transmission is plotted in Figure 9 and then in Figure 9a  $v_2 > v_1$  we distinguish five different zones characterizing the behavior of the transmission. Indeed, the first zone is determined by the greater effective mass, namely  $\epsilon l_B < k_y l_B + \frac{d_1}{l_B}$ . The second zone identifies with the lower Klein energy zone characterized by resonances in the interval  $k_y l_B + \frac{d_1}{l_B} < \epsilon l_B < v_1 l_B$ .

Here we have full transmission at some specific energies despite the fact that the particle energy is less than the height of the barrier. As  $d_1/l_B$  increases, the oscillations in the Klein zone get reduced. This strong reduction in the transmission in the Klein zone seem to suggest the potential suppression of Klein tunneling as we increase the width of the well region,  $d_1/l_B$ . The third zone  $v_1 l_B < \epsilon l_B < v_2 l_B - k_y l_B - \frac{\mu l_B}{2}$  is a window where the transmission oscillates around the value of the full transmission. The fourth zone defined by  $v_2 l_B - k_y l_B - \frac{\mu l_B}{2} < \epsilon l_B < v_2 l_B + k_y l_B + \frac{\mu l_B}{2}$  is a window where the transmission is almost zero. The fifth zone  $\epsilon l_B > v_2 l_B + k_y l_B + \frac{\mu l_B}{2}$  contains oscillations, the transmission converges towards unity. Contrary to the case  $v_1 > v_2$ , the situation where  $v_2 > v_1$  is shown in Figure 9b we distinguish four different zones characterizing the behavior of the transmission. Indeed, compared to Figure 9a, the behavior in the first zone is the same. Concerning the zones  $k_y l_B - \frac{d_1}{l_B} < \epsilon l_B < v_2 l_B - k_y l_B - \frac{\mu l_B}{2}$  and  $v_2 l_B + k_y l_B + \frac{\mu l_B}{2} < \epsilon l_B < v_1 l_B$  the transmission oscillates similarly to Figure 9a. In the zone  $v_2 l_B - k_y l_B - \frac{\mu l_B}{2} < \epsilon l_B < v_2 l_B + k_y l_B + \frac{\mu l_B}{2}$ , one can see that both curves start from zero transmission and oscillate while the valley gets wider as  $d_1/l_B$  decreases. Finally zone  $\epsilon l_B > v_1 l_B$  the transmission oscillate to reach full transmission asymptotically.

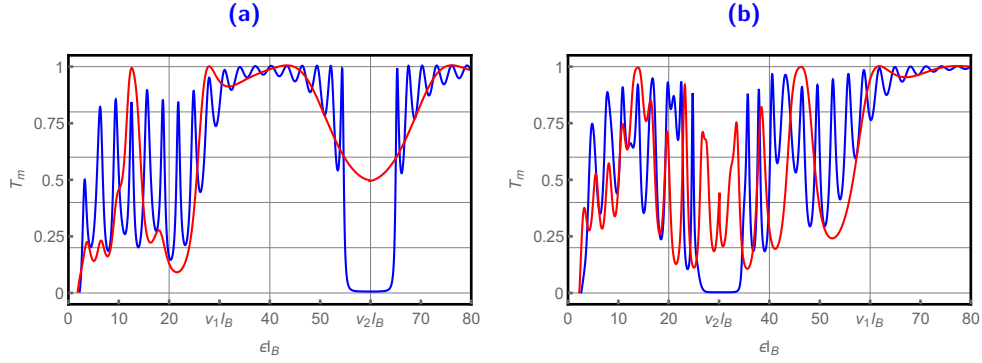


**Figure 9** – (color online) Transmission probability  $T_m$  for the magnetic barrier as a function of energy  $\epsilon l_B$  with  $\frac{d_1}{l_B} = 0.1$  (red color),  $\frac{d_1}{l_B} = 0.5$  (blue color),  $\frac{d_2}{l_B} = 1.5$ ,  $\mu l_B = 4$  and  $k_y l_B = 2$ . (a):  $v_1 l_B = 30$ ,  $v_2 l_B = 60$ . (b):  $v_1 l_B = 60$ ,  $v_2 l_B = 30$ .

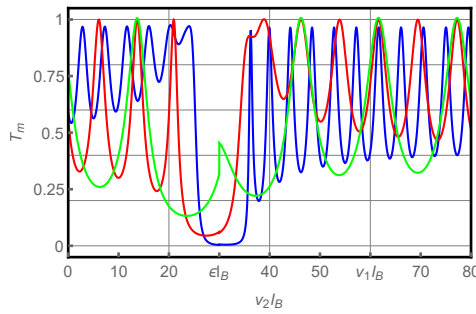


**Figure 10** – (Color online) Transmission probability  $T_m$  for the magnetic barrier as a function of the potential  $v_2 l_B$  with  $\frac{d_1}{l_B} = 0.1$  (green color),  $\frac{d_1}{l_B} = 0.2$  (red color),  $\frac{d_1}{l_B} = 0.34$  (blue color),  $\frac{d_2}{l_B} = 1.5$ ,  $\mu l_B = 4$ ,  $k_y l_B = 2$ ,  $v_1 l_B = 60$  and  $\epsilon l_B = 30$ .

It is worth analyzing the transmission versus the potential  $v_2 l_B$ . In doing so, we choose a fixed value of  $d_1/l_B$  as shown in Figure 10. It is clear that as we increase the well width  $d_1/l_B$ , hence for a fixed  $v_1 l_B$  and  $d_2/l_B$  we will be increasing the strength of the electrostatic field, the number of oscillations increases and a zero transmission region appears.

## 5 Conclusion

We have considered a model that describes electron transmission in monolayer graphene through a triangular electrostatic double barriers in the presence of a magnetic field localized in the well region. To investigate the transport properties of our system, we have considered separately the two effects: first we considered an electrostatic double barrier alone then we added a uniform magnetic field effect in the well region. In both cases, we have investigated analytically and numerically the transmission probability. This has been achieved through solving the corresponding eigenvalue equation which resulted in the energy spectrum in terms of different physical parameters that control the system Hamiltonian.

Using the continuity of the wavefunctions at the interfaces between different regions inside and outside the barriers we have ensured conservation of the local current density and derived the relevant transport coefficients of the present system. Specifically, using the transfer matrix method, we have deduced the corresponding transmission coefficient and determined how the transmission probability is affected by various physical parameters. In particular for the electrostatic double barrier in the absence of magnetic field, the resonances were seen to appear in different Klein tunneling regions. A gap region appeared for energies around the value of the elevated well potential, independently of the strength of the electrostatic field.

Subsequently, we have analyzed the same system but this time taking into account the presence of a static magnetic field localized in the well region. Using boundary conditions, we have split the energy space into three domains and then calculated the transmission probability in each domain. In each situation, we have discussed the transmission and resonances that characterize each region and stressed the importance of our results.

Our results indicate that the Klein paradox, full transmission close to normal incidence, persists for all values the electrostatic field or equivalently the double barrier-tilting angle. From the application point of view, our current investigation suggests that tunable filtering of Dirac electrons by an electrostatic double barrier is possible for near normal incidence at all values of the electrostatic field or tilting angle. This observation could be very beneficial in designing graphene based electronic lenses.

## Acknowledgments

The generous support provided by the Saudi Center for Theoretical Physics (SCTP) is highly appreciated. AJ and HB acknowledge the support of King Fahd University of Petroleum and minerals.

## References

- [1] K. S. Novoselov, A. K. Geim, S. V. Morozov, D. Jiang, Y. Zhang, S. V. Dubonos, I. V. Grigorieva and A. A. Firsov, *Science* 306, 666 (2004).
- [2] N. Stander, B. Huard and D. Goldhaber-Gordon, *Phys. Rev. Lett.* 102, 026807 (2009).
- [3] M. I. Katsnelson, K. S. Novoselov and A. K. Geim, *Nature Phys.* 2, 620 (2006).

- [4] H. Sevinçli, M. Topsakal and S. Ciraci, Phys. Rev. B 78, 245402 (2008).
- [5] M. Ramezani Masir, P. Vasilopoulos and F. M. Peeters, New J. Phys. 11, 095009 (2009).
- [6] L. Dell'Anna and A. De Martino, Phys. Rev. B 79, 045420 (2009).
- [7] S. Mukhopadhyay, R. Biswas and C. Sinha, Phys. Status Solidi B 247, 342 (2010).
- [8] E. B. Choubabi, M. El Bouziani and A. Jellal, Int. J. Geom. Meth. Mod. Phys. 7, 909 (2010).
- [9] H. Bahlouli, E. B. Choubabi, A. Jellal and M. Mekkaoui, J. Low Temp. Phys. 169, 51 (2012).
- [10] A. Jellal and A. El Mouhafid, J. Phys. A: Math. Theo. 44, 015302 (2011).
- [11] H. Bahlouli, E. B. Choubabi, A. El Mouhafid and A. Jellal, Solid State Communications 151, 1309 (2011).
- [12] A. El Mouhafid and A. Jellal, J. Low Temp. Phys. 173, 264 (2013).
- [13] A. Matulis, F. M. Peeters and P. Vasilopoulos, Phys. Rev. Lett. 72, 1518 (1994).
- [14] M. Ramezani Masir, P. Vasilopoulos and F. M. Peeters, Phys. Rev. B 82, 115417 (2010).
- [15] J. Tworzydło, B. Trauzettel, M. Titov, A. Rycerz and C. W. J. Beenakker, Phys. Rev. Lett. 96, 246802 (2006).
- [16] M. V. Berry and R. J. Modragon, Proc. R. Soc. London Ser. A 412, 53 (1987).
- [17] M. Abramowitz and I. Stegun, Handbook of Integrals, Series and Products, (Dover, New York, 1956).
- [18] L. Gonzalez-Diaz and V. M. Villalba, Phys. Lett. A 352, 202 (2006).